Science Bulletin 64 (2019) 1577–1583

Contents lists available at ScienceDirect

Science Bulletin

journal homepage: www.elsevier.com/locate/scib

Science Bulletin
www.scibull.com

Article

Storage of telecom-C-band heralded single photons with orbital-angular-momentum encoding in a crystal

Yi-Lin Hua [a,b,1], Tian-Shu Yang [a,b,1], Zong-Quan Zhou [a,b,*], Jian Wang [a,b], Xiao Liu [a,b], Zong-Feng Li [a,b], Pei-Yun Li [a,b], Yu Ma [a,b], Chao Liu [a,b], Peng-Jun Liang [a,b], Jun Hu [a,b], Xue Li [a,b], Chuan-Feng Li [a,b,*], Guang-Can Guo [a,b]

[a] CAS Key Laboratory of Quantum Information, University of Science and Technology of China, Hefei 230026, China
[b] CAS Center for Excellence in Quantum Information and Quantum Physics, University of Science and Technology of China, Hefei 230026, China

ARTICLE INFO

Article history:
Received 2 July 2019
Received in revised form 13 August 2019
Accepted 27 August 2019
Available online 9 September 2019

Keywords:
Quantum repeater
Quantum memory
Heralded single photons
Orbital angular momentum
Telecommunication band

ABSTRACT

A memory-based quantum repeater architecture provides a solution to distribute quantum information to an arbitrary long distance. Practical quantum repeaters are likely to be built in optical-fiber networks which take advantage of the low-loss transmission between quantum memory nodes. Most quantum memory platforms have characteristic atomic transitions away from the telecommunication band. A nondegenerate photon pair source is therefore useful for connection of a quantum memory to optical fibers. Here, we report a high-brightness narrowband photon-pair source which is compatible with a rare-earth-ion-doped crystal Pr^{3+}:Y_2SiO_5. The photon-pair source is generated through a cavity-enhanced spontaneous parametric down-conversion process with the signal photon at 606 nm and the idler photon at 1540 nm. Moreover, using the telecom C-band idler photons for heralding, we demonstrate the reversible transfer of orbital-angular-momentum qubit between the signal photon and the quantum memory based on Pr^{3+}:Y_2SiO_5.

1. Introduction

Interface between a non-classical state of light and matter system is a fundamental requirement for many quantum information processing protocols [1]. Quantum repeater [2], for instance, is one of typical applications which can overcome the exponential transmission loss of single photons and extend the distance of entanglement distribution. Quantum repeaters are based on many qubit-hosting nodes separated by dozens or a hundred of kilometers and quantum channels which transport flying qubits to establish entanglement between quantum nodes [3,4]. The flying qubits are tended to be carried by photons. To afford low-loss transmission, the quantum channels should be in the telecommunication wavelength range [5,6].

Though the telecom quantum memories exist, e.g., erbium doped solids [7,8], the current efficiency and storage time are severely limited. Most of the platforms that serve as quantum nodes operate with photons at visible to near infrared regime which is apart from the telecom window [9–11]. Approaches including quantum frequency conversion (QFC) [12] and employing nondegenerate photon-pair source [13,14] can both build a nonclassical correlation between a stationary quantum node and a flying telecom photon. QFC has already been demonstrated in various platforms including atomic gas [15–17], nitrogen vacancy (NV) defect in diamond [18,19], trap ions [20,21] and rare-earth-ion-doped crystals (REICs) [22]. Quantum entanglement between a telecom photon and a REIC Nd^{3+}:Y_2SiO_5 or a Ti:Tm:$LiNbO_3$ waveguide has also been demonstrated using the photon-pair source generated by spontaneous parametric down-conversion (SPDC) [23,24].

Compared to the quantum memory achieved via the materials of Nd^{3+}:Y_2SiO_5 or Ti:Tm:$LiNbO_3$, the quantum memory based on Pr^{3+}:Y_2SiO_5 has better performances in the storage efficiency and the storage time [25,26]. Particularly, it has the required energy levels for conducting a spin-wave storage for longer and programmable storage time [27,28]. To meet the requirements of this particular material, cavity enhanced nondegenerate narrowband photon-pair sources were created [14,29,30]. Nonclassical correlation between an E-band telecom photon with a collective optical excitation or a collective spin wave in Pr^{3+}:Y_2SiO_5 crystals has also been established by using the quantum light source [31,32].

* Corresponding authors.
E-mail addresses: zq_zhou@ustc.edu.cn (Z.-Q. Zhou), cfli@ustc.edu.cn (C.-F. Li).
[1] These authors contributed equally to this work.

https://doi.org/10.1016/j.scib.2019.09.006
2095-9273/

The C-band photon has lower loss in fiber delivery compared to the E-band photon and is preferable for long-distance transmission. Therefore, in this paper, we report a praseodymium-based memory-compatible narrowband photon-pair source with C-band heralding photons. A single cluster spectral distribution and a high spectral brightness are observed of the quantum light source owing to cavity configuration with the type-0 quasi-phase-matching crystal. Furthermore, we demonstrate the quantum storage of heralded single-photon orbital-angular-momentum (OAM) qubit in a Pr^{3+}:Y_2SiO_5 crystal. Using the OAM degree of freedom of photons, it is promising to carry more quantum information owing to its high-dimensional property [33]. Although storage of OAM qubit or entanglement in OAM degree of freedom has been proven experimentally [34–36], the lacking of telecom heralding photons in these experiments [34–36] reduces the practicality of the quantum memories for quantum repeaters. The current work combines advantages of high-capacity information encoding by using OAM and C-band heralding for directly interfacing with telecom fibers, which can both enhance the data rate for the memory-based quantum network.

2. Creation of the cavity-enhanced single-photon source

The schematic diagram of the single-photon source is shown in Fig. 1. The laser at 606 nm is frequency-stabilized to a high-finesse cavity which ensures a spectral bandwidth of below 10 kHz, whose center frequency is compatible with the $^3H_4$ – $^1D_2$ transition of Pr^{3+}:Y_2SiO_5. This narrowband laser forms the basis for all the following processes of cavity length locking and the frequency stabilizing of another laser at 1540 nm. The pump light for the nondegenerate narrowband photon-pair source has a wavelength of 434.8 nm which is produced from a sum-frequency generation process instead of using an ultraviolet laser directly. The sum-frequency generation is accomplished by using a 2 cm-long periodically poled lithium-niobate (PPLN) waveguide (WG, HCPhotonics Corp).

The cavity-enhanced parametric-down-conversion process [37] is mainly composed of a 2-cm long PPLN crystal with type 0 quasi-phase-matching condition and a bow-tie cavity. The cavity and the crystal therein give a free spectral range (FSR) of approximately 340 MHz. The cavity has three mirrors (M2, M3 and M4) with high reflectivity for both target wavelengths (up to 99.95% for 606 and 1540 nm) and another output coupling mirror M1 with a reflectivity of 98%. Anti-reflection coating for all these mirrors at 434.8 nm ensures a high transmittance (>95%) of the pump light. Both of the 606 and 1540 nm photons should be resonated with the cavity to enhance the generation rate. This is achieved by the following procedures. Two reference beams with target wavelengths are coupled into the cavity individually using different lens groups. The transmitted signal of the 606 nm reference beam detected by the photodetector 1 (PD1) is used to lock the cavity length through the M2 mirror controlled by a piezoelectric ceramics. The electro-optic modulator (EOM) in this path is used to generate sideband for the Pound-Drever-Hall locking technology [38]. The transmitted signal of the 1540 nm light from the cavity is detected by photodetector 2 (PD2), thus stabilizing its frequency through the self-contained module of the laser. The pump light is coupled into the cavity through M3 mirror. The generated photon pairs escape the cavity from M1 mirror which is copropagating with the reflections of the reference beams.

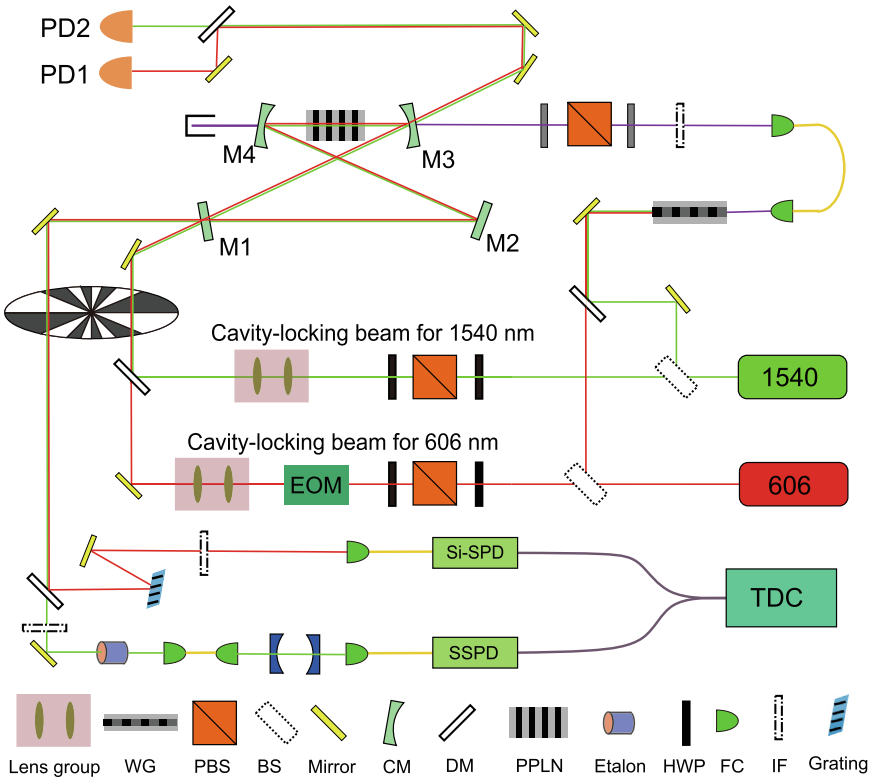

Fig. 1. (Color online) Diagram of the experimental setup of the cavity-enhanced SPDC. The pump light is generated through a sum-frequency generation process and connected to the cavity through an SMF. The polarization beam splitter (PBS) and half wave plates (HWPs) control the polarization of the pump light. Two reference beams at two wavelengths are combined with a DM. The lens groups in the two paths accomplish the mode matching to the cavity of the two wavelengths. Meanwhile, the lens groups also focus the two beams at the same position where the optical chopper is placed. In fact, when the signal and idler photons escape from the cavity through M1 mirror, there are also a series of lens (not shown on the figure) which make the photon pairs focus at another side of the chopper. The chopper works with a frequency of 200 Hz to separate the photon pairs from the reference beams. The photon pairs are then divided by another DM and coupled into SMFs for connection into single-photon-detectors.

Therefore, the next essential step is separating the photon-pair source from the classical reference beams. An optical chopper is introduced to isolate the photon pairs with reference beams and protect the single-photon-detectors. The reference beams with two target wavelengths are focused at a common position where the chopper is placed and the photon pairs are focused at another side of the chopper. The chopper separates the photon pairs from the reference beams through alternately letting the reference beams or photon pairs pass. It works with a duty cycle of 4:6. That is, the locking system works for a 40% time and the measurement time occupies a 60% time of the experimental sequence.

The signal and idler photons are separated by the dichroic mirror (DM) which has a high transmittance at the wavelength of 1540 nm and high reflectivity at the wavelength of 606 nm. Band-pass filters are employed to restrict the bandwidth of the signal and the idler photons to approximately 3 nm. The signal photons are then reflected by a Bragg grating with a full width at half maximum (FWHM) of approximately 10 GHz and then detected by a Silicon single-photon-detector (Si-SPD, detection efficiency approximately 60%). The total transmission loss between the output coupling mirror and the single-photon-detector is approximately 30%, which is measured using the signal reference beam. The idler photons are filtered by a 700-MHz etalon (FSR ≈ 30 GHz) and then coupled into a single mode fiber (SMF) for spatial mode cleaning. The output of the SMF passes through a home-made Fabry-Perot cavity and is then detected by a superconducting single-photon-detector (SSPD, detection efficiency approximately 35%). The filter cavity is continuously locked by another beam at 606 nm. When the filter cavity is locked, it has a linewidth of approximately 30 MHz and a transmittance of 80% at 1540 nm. The total transmission loss between the output coupling mirror of the bow-tie cavity and the single-photon-detector is approximately 58% considering the transmission loss and the fiber coupling efficiencies before and after the filter cavity, which is also measured using the idler reference beam.

3. Quantum characteristics of the single-photon source

The quantum characteristics of the photon pairs can be analyzed by time-correlated measurements, typically, through the second-order cross-correlation function $G^2_{s,i}$. The normalized form of $G^2_{s,i}$ can be expressed as [3,23]:

$$g^2_{s,i} = \frac{\langle E_s^+(t) E_i^+(t+\tau) E_i(t+\tau) E_s(t)\rangle}{\langle E_i^+(t+\tau) E_i^+(t+\tau)\rangle \langle E_s^+(t) E_s(t)\rangle}, \quad (1)$$

where $E^+_{s,i}$ and $E_{s,i}$ are the electric field creation and annihilation operators for the signal and idler fields. It is widely known that the photon pairs emitted from the cavity consists of multiple spectral modes, despite that the nondegenerate parametric process have reduced photon-pair generation probability to limited clusters, each of which consists of several longitudinal modes [14]. To explore this multiple-mode property, the Bragg grating, etalon and the filter cavity are removed. The signal and idler photons are separately filtered by band-pass filters and then coupled into the SMFs for detection. To obtain a high timing resolution, both the signal and idler photons are sent to two SSPDs and their arrival times are recorded by the time-to-digital converter (TDC Picoquant 400). The coincidence dependence on the arrival-time difference (τ) is shown in Fig. 2a.

The outline of the curve gives a FWHM correlation time of approximately 90 ns which indicating that the single mode biphoton bandwidth of 2.45 MHz. By fitting the function $\exp(-2\pi\Delta\nu t)$ on the two sides of the outline of this figure, we can infer a spectral bandwidth of 2.15 MHz for the signal photons and 2.84 MHz for the idler photons. The escape efficiencies are estimated to be approximately 54% and 34% for the signal photons and idler photons since the internal round trip loss can be inferred through the bandwidths and FSR of the cavity [29]. However, neighboring modes of the state make the figure presents a comb-like structure. The insert figure intercepts a 30 ns interval of the $G^2_{s,i}(\tau)$ measurement where we can clearly see that these peaks have a period of 2.94 ns which corresponds to the FSR of 340 MHz of the bow-tie cavity.

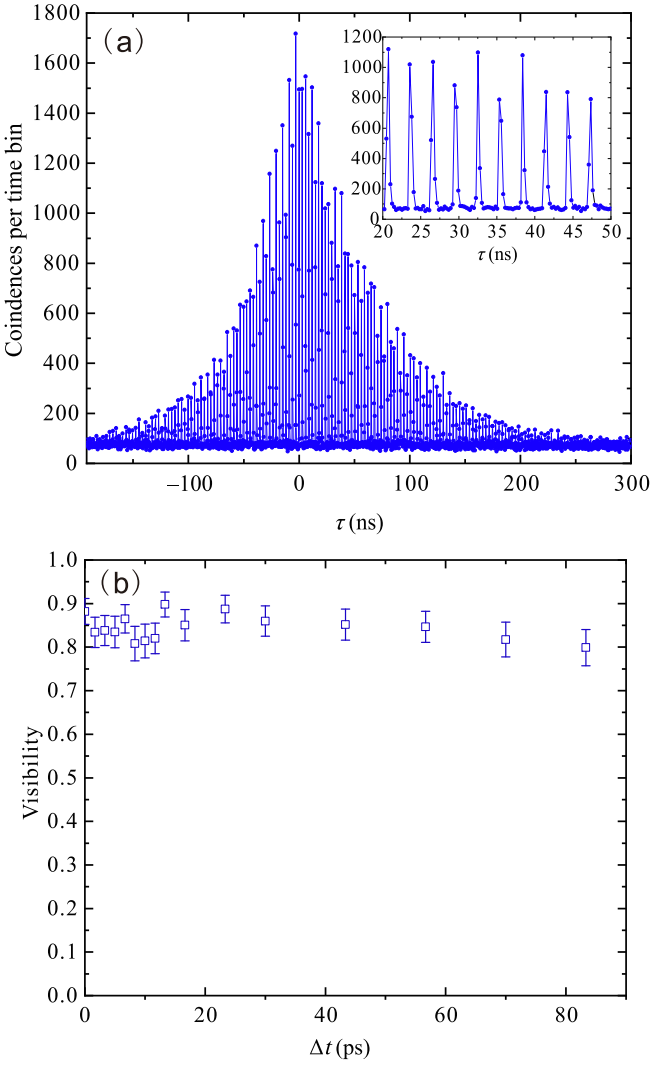

Fig. 2. (Color online) Quantum characteristics of the multiple-mode state. (a) Measured correlation function $G^2_{s,i}(\tau)$ of the multiple-mode state. The figure is measured at the pump power of 1 mW with a bin size of 256 ps and an integration time of 300 s. The inset is a zoom to 20–50 ns window. (b) $|g^{(1)}_s(\Delta t)|$ measurement result of this multiple-mode state.

Compared to the degenerate cavity-enhanced SPDC state, the two wavelengths we choose are quite different so that the FSRs have a little difference. Therefore, the state is typically consisted of several clusters considering the phase matching condition [39,40]. The cluster effect can be analyzed by exploring the first order autocorrelation (coherence) function $V = |g^{(1)}_s(\Delta t)|$ of the signal photons heralded by the idler photons [41]. A Michelson interferometer is built for signal photons before the optical fiber. We first examine the performance of this interferometer by scanning the length of one arm of the interferometer in a range of 15 mm range (corresponds to a time of 100 ps) with a precision of 0.5 mm. The reference classical light gets a near unity visibility

so the interferometer is reliable. When the heralded signal photons are put to tests, the visibility is shown in Fig. 2b. We find that the visibilities remain above 80% without oscillations observed in an interval of 100 ps. No oscillations observed in the figure indicate that there is only one cluster surviving of this multiple-mode state. It may be attributed to the slight difference of the FSRs between the signal and idler field that leads to an ultra-wide cluster spacing [40]. The unique cluster is also beneficial to the following process of extracting the single longitudinal mode from the multiple-mode state.

In absence of the frequency multiplexing operation of the quantum memory [42], the multiple-mode state cannot be applied directly. Most of the current experiments of spin-wave storage only support light sources with bandwidths of approximately 3 MHz [27,28]. Therefore, a single mode operation achieved of the photon-pair source is more important. It can be simply realized by putting back of the Bragg grating, etalon and the filter cavity. A filter cavity in cooperation with the etalon for the idler photons can guarantee the coincident counts consisted of only one longitudinal mode, but the huge unilateral counts of signal photons cause massive random coincidences that influence the result of the time-correlated measurement. So, a Bragg grating is placed before the SMF for signal photons to reduce the unilateral counts. The memory crystal can further suppress the unilateral counts completely in the practical application of interfacing the light source with the quantum memory [31,32].

The second-order cross-correlation function of single-mode state is shown in Fig. 3a. A cross-correlation function with an 8-ns bin size and 256-ps bin size (inset figure) are both measured at the pump power of 1 mW. From the inset figure we can find the oscillation at the 2.94-ns period disappears which proves that the neighboring modes are removed by our filtering operation. The $g^2_{s,i}(0)$ value is 13.73 ± 0.9 (measured in a time window of 32 ns). Due to the fact that signal photons (or idler photons) itself exhibits photon statistics typical of thermal light, so that the autocorrelation function should be less than 2 [43]. So the non-classicality is proved to measure the $g^2_{s,i}(0)$ value greater than 2 and the current state exceeds the classical limit [44,45]. The memory crystal can be employed to remove other modes of the signal photons by spectrally preparing a transparent window with a bandwidth of several MHz through spectral hole burning so that a higher $g^2_{s,i}(0)$ value will be expected [28,31,32].

A higher value of $g^2_{s,i}(0)$ can also be obtained by reducing the pump power to decrease the creation rate of multiphoton emission. We measure the $g^2_{s,i}(0)$ values as well as the coincidence rate at different pump powers. The results are shown in the Fig. 3b without subtracting any background counts. $g^2_{s,i}(0)$ value decreases with the increasing pump power and the coincidence rate has an opposite trend. A $g^2_{s,i}(0)$ value of 33 ± 2.9 has been obtained at pump power of 200 μW. The result with lower pump power is not measured considering the dark counts. Moreover, we obtained a normalized spectrum brightness of approximately 25.3 photon pairs/(s·mW·MHz) which is more than two times brighter than the result in Ref. [29]. This high brightness is mainly benefited from the type 0 quasi-phase-matching.

The heralding efficiency is another important technical indicator of the photon source for practical applications. The heralding efficiency is defined as $\eta = \frac{P_{s,i}}{P_i \eta_{det,s}}$, where $P_{s,i}$ and P_i is coincidence probability and the probability to detect a herald photon. $\eta_{det,s}$ is the detection efficiency of the Si-SPD for signal photons. In our experiment, η is 17.5% ± 0.2% at the pump power of 1 mW. The heralding efficiency is primarily limited by the escape efficiency and transmission loss of the signal photons. Besides, the wider bandwidth of the idler photons compared to that of the signal photons may also restrict the heralding efficiency. It can be improved by slightly changing the reflectivity of M1 mirror to achieve similar bandwidths of the two wavelengths.

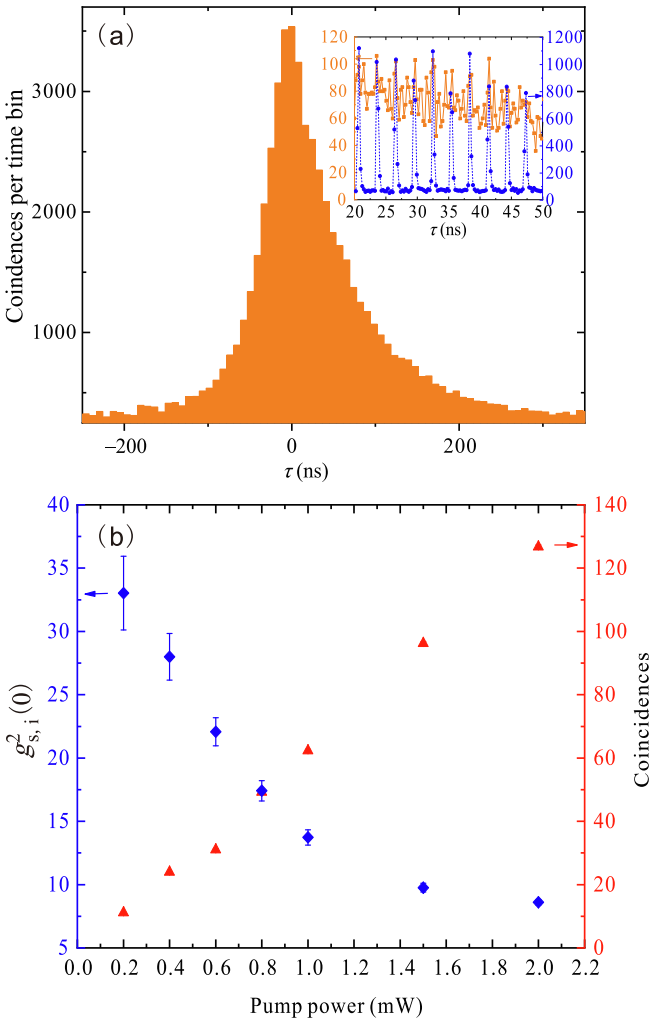

Fig. 3. (Color online) Quantum characteristics of the single-mode state. (a) Measured correlation function $G^2_{s,i}(\tau)$ of the single-mode state. The figure is measured at the pump power of 1 mW with a bin size of 8.192 ns. The integration time is 1200 s. The inset is a zoom to 20–50 ns regime with a bin size of 256 ps. As a comparison, we also show the result (blue dashed line) of the multiple-mode state measured in Fig. 2a. (b) The pump-power dependence of the $g^2_{s,i}(0)$ value and the coincidence rate.

4. Storage of photonic OAM qubit

The interface between the single-photon source and the quantum memory is the basis of construction of a quantum-repeater-based network. Here, we choose the OAM of photons to encode quantum information. This degree of freedom has shown great opportunity for high dimensional encoding and large multimode capacity in a multiplexed quantum memory [33,46–48]. The capacity of storing temporal or spectral modes will be restricted by the bandwidth and absorption depth of the memory, but there are no such limitations when the quantum memory is multiplexed using the spatial modes, e.g., the OAM [36]. We present the experimental realization of storing heralded OAM qubit in the memory crystal (MC), as shown in Fig. 4a. The MC in this experiment is a 6-mm-thick Pr^{3+}:Y_2SiO_5 crystal (Pr^{3+} concentration of 0.05%) whose inhomogeneous linewidth is approximately 5 GHz. The pump power of the photon-pair source is 2 mW in the following

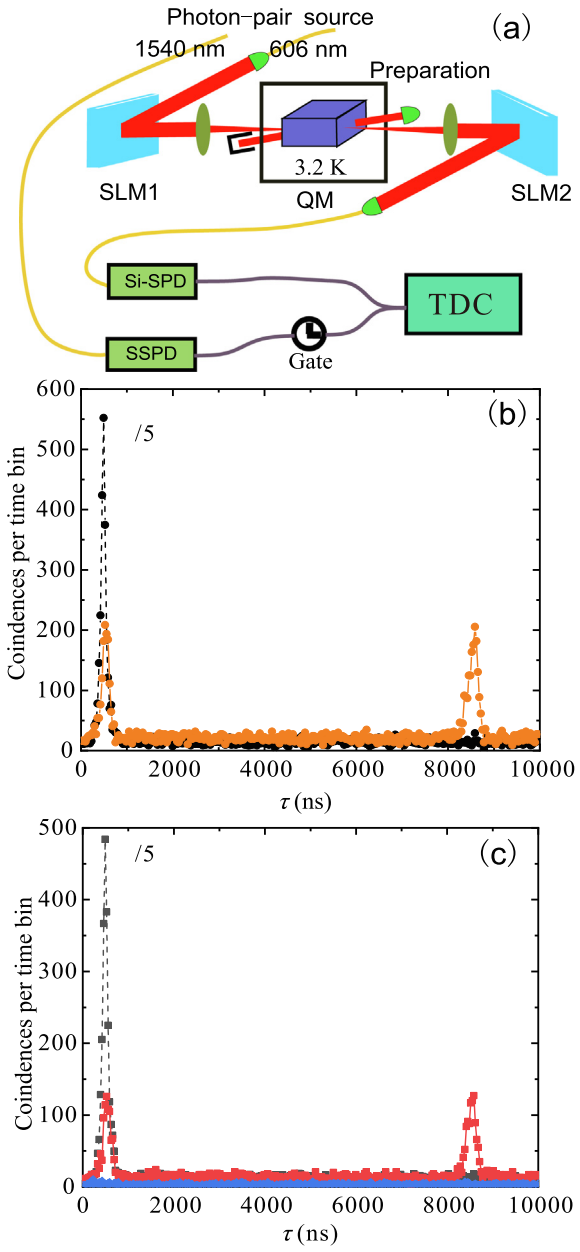

Fig. 4. (Color online) Storage of heralded photonic OAM qubit. (a) The schematic of storing heralded OAM qubit in a Pr^{3+}:Y_2SiO_5 crystal. The AFC preparation time is approximately 300 ms in an experimental cycle of 713 ms. The arrival time of retrieved signal photons and idler photons are recorded by a TDC. The measurement time is 325 ms in each experimental cycle after the AFC is prepared. An electric gate (Ortec model 935) is placed after the SSPD to eliminate the noise of the coincidences. The gate is off during the AFC preparation or implementation of the locking system. (b) The coincidence histogram heralded by idler photons when the signal photons are encoded with the mode $|LG_{p=0}^{l=0}\rangle$ using SLM1. Black dotted line is the result (divided by 5 times) that signal photons pass through a transparency window and the orange solid line represents the result that signal photons go through a 4-MHz AFC. The SLM2 is set with the same mode as input state. (c) The coincidence histogram heralded by idler photons when the signal photons are encoded with the superposition state of $\frac{|L\rangle+|R\rangle}{\sqrt{2}}$ using SLM1. Black dotted line is the result (divided by 5 times) that signal photons pass through a transparency window and the red solid line represents the result that signal photons go through an AFC. In the above two situations, the SLM2 is set with the same mode as the input state. The line marked with blue diamonds is the result that signal photons pass through an AFC while the SLM2 is set with the mode $\frac{|L\rangle-|R\rangle}{\sqrt{2}}$.

experiment. To check the compatibility of the photon-pair source with the MC, we create a 12-MHz-wide transparency window in the memory crystal. The signal photons are sent to this transparency window and the coincidence histogram heralded by the idler photons is measured. The FWHM of correlation time between the telecom photons and signal photons is approximately 105 ns (as seen from the black curve in Fig. 4b), leading to a biphoton bandwidth of 2.1 MHz [29]. The decreasing of the biphoton bandwidth may due to the fact that the memory crystal with a 12-MHz-wide transparency window does not contain all the frequency components of the signal photons completely. But considering the transmission loss of the signal photons, we infer that the 12-MHz-wide transparency window extracts most signal photons of the central mode, so this result can be used as an input trace.

The atomic frequency comb (AFC) [49] protocol is employed to store the heralded single photons. A 4-MHz AFC is created in the MC with a periodicity $\Delta = 125$ kHz, which introduces a programmed storage time $\tau_{AFC} = 1/\Delta = 8$ μs. The preparation procedure of the AFC is described in Refs. [28,42]. The signal photons are first encoded with Laguerre-Gaussian (LG) mode $|LG_{p=0}^{l=0}\rangle$ [34] by the spatial light modulator 1 (SLM1) and the spatial light modulator 2 (SLM2) is set to mode $|LG_{p=0}^{l=0}\rangle$ as well. The coincidence histogram before and after storage are recorded in Fig. 4b, which is measured with a bin size of 32 ns and an integration time of 3000 s. By comparing the coincidences of AFC echo to the counts of the input state, we obtain a memory efficiency $\eta_{AFC} = 12.6\%$. Bandwidth matching degree between the AFC (total width of 4 MHz) and the input photons is estimated as 85%.

To prove the non-classical correlation between the signal photon and the telecom C-band idler photon during the storage process, the correlations between the signal photon and the idler photon are measured by the normalized second-order cross-correlation function $g_{s,i}^2$ value before and after the storage process. The measurement results are shown in Fig. 4b. For the transmitted signal photon from the transparency window, the $g_{s,i}^2$ value is estimated to be 41.3 ± 1.1, which is significantly greater than the classical bound of 2. This $g_{s,i}^2$ value also leads to an upper bound of the autocorrelation of heralded signal photon to be $g_{i|s,s}^2 \leq 0.095$ [45], which indicating that the photon source itself is closed to the ideal single photons ($g_{i|s,s}^2 = 0$). Compared to the photon source that the signal photons are unfiltered to single longitudinal mode, the $g_{s,i}^2$ value rises significantly due to the filtering effect of the memory crystal, though the signal-photon loss during transmission reduces the value to a certain extent. The $g_{i|s,s}^2$ value can be further decreased through reducing the pump power of the single photon source, but it will lead to low photon counting rate that is disadvantage to the application in quantum communications. Further enhancing the photon rate and the quality of correlation are required for practical applications such as the quantum repeater. The correlation between the retrieved signal photon and the idler photon is $g_{echo,i}^2$, which has a value of approximately 11.4 ± 0.4 after a storage time of 8 μs. The drop of the $g_{s,i}^2$ value is mainly due to the low recall efficiency of the memory. The upper bound of the autocorrelation of the heralded AFC echo is 0.175, which demonstrates that the quantum memory well preserved the single-photon statistics.

A superposition OAM qubit state of $\frac{|L\rangle+|R\rangle}{\sqrt{2}}$ is then encoded into the signal photons using SLM1, where $|L\rangle$ ($|R\rangle$) is defined as LG modes $|LG_{p=0}^{l=+1}\rangle$ ($|LG_{p=0}^{l=-1}\rangle$). SLM2 is set to $\frac{|L\rangle+|R\rangle}{\sqrt{2}}$ or $\frac{|L\rangle-|R\rangle}{\sqrt{2}}$ to benchmark the memory performance of maintaining the coherence of encoded quantum information. This is achieved by assessing the visibility of the readout state, which is defined as $\frac{p_+-p_-}{p_++p_-}$ where $p_\pm$ is the probabilities of detecting readout photons with states of $\frac{|L\rangle\pm|R\rangle}{\sqrt{2}}$. The measured results are shown in Fig. 4c, which use the same bin size and

integration time as Fig. 4b. We observe a memory efficiency of $\eta_{AFC} = 8.5\%$ for the OAM qubit state $\frac{|L\rangle+|R\rangle}{\sqrt{2}}$ and $g^2_{echo,i} = 10.9 \pm 1.1$. The decrease of the efficiency is mainly owing to the fact that the OAM qubit state $\frac{|L\rangle+|R\rangle}{\sqrt{2}}$ has a larger beam diameter than that of the mode $\left|LG^{l=0}_{p=0}\right\rangle$. Since the preparation beam has a limited diameter at memory crystal, when a good overlap with the mode $\left|LG^{l=0}_{p=0}\right\rangle$ is achieved, it may result in imperfect pump effect for the mode $\frac{|L\rangle+|R\rangle}{\sqrt{2}}$. This limitation can be overcome by increasing the beam diameter or using a super-Gaussian spatial profile for the preparation light [36]. Moreover, the measured visibility of the AFC echo is 94.0%±1.1%, which indicates that the coherence of the superposition state is maintained well during the storage process.

In this experiment, a heralded single photon encoded with OAM qubit is stored as a collective optical excitation with a predetermined delay. We note that the similar cavity enhanced photon sources have been stored as a collective optical excitation and a spin excitation by another group [31,32]. There are some technical promotions about the quantum light source in this experiment. The telecom C-band idler photon is used to herald the existence of signal photon, which is more compatible with fiber network compared to the E-band idler photons. Besides, a single cluster and a higher spectral brightness of the single photon source are observed in our experiment, which make our source more superior and convenient for single-mode applications. Ref. [22] shows the capability of converting the memory compatible photons to telecom C-band photons through a nonlinear waveguide, but the overall conversion efficiency of the device is restricted. From this aspect, our work is the first combination of the advantages of high-capacity information encoding by using OAM and C-band heralding for directly interfacing with telecom fiber network in a single experiment.

Our work can also be extended to store a heralded single photon as a spin wave by applying two control pulses which enables an on-demand readout. However, using this approach, the pump power of the source should be reduced and the transmission loss of signal photons during the storage process should be controlled to improve the second-order cross-correlation function and the heralding efficiency. In addition, the noise caused by the control pulses should be effectively suppressed to ensure the final signal-to-noise ratio [28,32]. The probabilistic single photon source in our experiment can therefore be converted to a deterministic source by storing the heralded single photon in a memory cell and releasing it when needed. Besides, the temporal and/or spectral multimode operations are widely implemented in the AFC protocol based on REICs [28,50–52]. These DOFs of photons are independent with photonic OAM, so that the spatial mode encoding in our experiment can be parallelly utilized with temporal mode encoding and frequency mode encoding [42], which will greatly enhance the capacity of a quantum memory and the data rate of a quantum repeater.

5. Conclusion

In conclusion, we have prepared a C-band telecom heralded single-photon source with a high brightness which is compatible to the state-of-art quantum memory based on Pr^{3+}:Y_2SiO_5. Using the AFC protocol, we prove non-classical correlation between a collective excitation of the memory crystal and a telecom photon. By employing OAM encoding of the signal photons, we demonstrate the reliable storage of superposition qubit state heralded by C-band telecom photons.

The current protocol can combine with spin-wave storage to extend the memory time and achieve an on-demand readout, given that the storage time of 8 μs can already enable the generation of an entanglement between two quantum memories with a distance of several kilometers. A promising approach of entanglement generation is creating OAM entanglement of narrowband photon-pair source. The signal photons can be stored by the quantum memory [34,42] while the telecom photons can be transmitted through few-mode fiber [53] or free space [48,54] to establish high-dimensional entanglement between remote ensembles.

Conflict of interest

The authors declare that they have no conflict of interest.

Acknowledgments

This work was supported by the National Key R&D Program of China (2017YFA0304100), the National Natural Science Foundation of China (61327901, 11774331, 11774335, 11504362, 11821404, and 11654002), Anhui Initiative in Quantum Information Technologies (AHY020100), Key Research Program of Frontier Sciences, CAS (QYZDY-SSW-SLH003), and the Fundamental Research Funds for the Central Universities (WK2470000023, WK2470000026). We also thank Dr. Zhi-Yuan Zhou for discussions and technical support.

Author contributions

Supervised by Profs. Zong-Quan Zhou and Chuan-Feng Li, Yi-Lin Hua and Tian-Shu Yang built the experimental setup, analyzed the data and wrote the paper. All the authors contributed to the conception and the analysis of the experiment.

References

[1] Hammerer K, Sørensen AS, Polzik ES. Quantum interface between light and atomic ensembles. Rev Mod Phys 2010;82:1041–93.
[2] Briegel H-J, Dür W, Cirac JI, et al. Quantum repeaters: the role of imperfect local operations in quantum communication. Phys Rev Lett 1998;81:5932.
[3] Sangouard N, Simon C, de Riedmatten H, et al. Quantum repeaters based on atomic ensembles and linear optics. Rev Mod Phys 2011;83:33–80.
[4] Simon C, de Riedmatten H, Afzelius M, et al. Quantum repeaters with photon pair sources and multimode memories. Phys Rev Lett 2007;98:190503.
[5] Nagayama K, Kakui M, Matsui M, et al. Ultra-low-loss (0.1484 dB/km) pure silica core fibre and extension of transmission distance. Electron Lett 2002;38:1168–9.
[6] Yin HL, Chen TY, Yu ZW, et al. Measurement-Device-Independent quantum key distribution over a 404 km optical fiber. Phys Rev Lett 2016;117:190501.
[7] Lauritzen B, Minar J, de Riedmatten H, et al. Telecommunication-wavelength solid-state memory at the single photon level. Phys Rev Lett 2010;104:080502.
[8] Saglamyurek E, Jin J, Verma VB, et al. Quantum storage of entangled telecom-wavelength photons in an erbium-doped optical fibre. Nat Photonics 2015;9:83–7.
[9] Kimble HJ. The quantum internet. Nature 2008;453:1023–30.
[10] Pfister AD, Salz M, Hettrich M, et al. A quantum repeater node with trapped ions: a realistic case example. Appl Phys B 2016;122:89.
[11] Togan E, Chu Y, Trifonov AS, et al. Quantum entanglement between an optical photon and a solid-state spin qubit. Nature 2010;466:730–4.
[12] Kumar P. Quantum frequency conversion. Opt Lett 1990;15:1476–8.
[13] Bussières F, Clausen C, Tiranov A, et al. Quantum teleportation from a telecom-wavelength photon to a solid-state quantum memory. Nat Photonics 2014;8:775–8.
[14] Fekete J, Rielander D, Cristiani M, et al. Ultranarrow-band photon-pair source compatible with solid state quantum memories and telecommunication networks. Phys Rev Lett 2013;110:220502.
[15] Dudin YO, Radnaev AG, Zhao R, et al. Entanglement of light-shift compensated atomic spin waves with telecom light. Phys Rev Lett 2010;105:260502.
[16] Radnaev AG, Dudin YO, Zhao R, et al. A quantum memory with telecom-wavelength conversion. Nat Phys 2010;6:894–9.
[17] Farrera P, Maring N, Albrecht B, et al. Nonclassical correlations between a C-band telecom photon and a stored spin-wave. Optica 2016;3:1019.
[18] Dréau A, Tcheborateva A, Mahdaoui AE, et al. Quantum frequency conversion of single photons from a Nitrogen-Vacancy center in diamond to telecommunication wavelengths. Phys Rev Appl 2018;9:064031.

[19] Ikuta R, Kobayashi T, Yasui S, et al. Frequency down-conversion of 637 nm light to the telecommunication band for non-classical light emitted from NV centers in diamond. Opt Express 2014;22:11205–14.
[20] Bock M, Eich P, Kucera S, et al. High-fidelity entanglement between a trapped ion and a telecom photon via quantum frequency conversion. Nat Commun 2018;9:1998.
[21] Walker T, Miyanishi K, Ikuta R, et al. Long-distance single photon transmission from a trapped ion via quantum frequency conversion. Phys Rev Lett 2018;120:203601.
[22] Maring N, Lago-Rivera D, Lenhard A, et al. Quantum frequency conversion of memory-compatible single photons from 606 nm to the telecom C-band. Optica 2018;5:507.
[23] Clausen C, Usmani I, Bussieres F, et al. Quantum storage of photonic entanglement in a crystal. Nature 2011;469:508–11.
[24] Saglamyurek E, Sinclair N, Jin J, et al. Broadband waveguide quantum memory for entangled photons. Nature 2011;469:512–5.
[25] Hedges MP, Longdell JJ, Li Y, et al. Efficient quantum memory for light. Nature 2010;465:1052–6.
[26] Heinze G, Hubrich C, Halfmann T. Stopped light and image storage by electromagnetically induced transparency up to the regime of one minute. Phys Rev Lett 2013;111:033601.
[27] Afzelius M, Usmani I, Amari A, et al. Demonstration of atomic frequency comb memory for light with spin-wave storage. Phys Rev Lett 2010;104:040503.
[28] Gundogan M, Ledingham PM, Kutluer K, et al. Solid state spin-wave quantum memory for time-bin qubits. Phys Rev Lett 2015;114:230501.
[29] Rieländer D, Lenhard A, Mazzera M, et al. Cavity enhanced telecom heralded single photons for spin-wave solid state quantum memories. New J Phys 2016;18:123013.
[30] Rieländer D, Lenhard A, Farìas OJ, et al. Frequency-bin entanglement of ultra-narrow band non-degenerate photon pairs. Quantum Sci Technol 2018;3:014007.
[31] Rielander D, Kutluer K, Ledingham PM, et al. Quantum storage of heralded single photons in a praseodymium-doped crystal. Phys Rev Lett 2014;112:040504.
[32] Seri A, Lenhard A, Rieländer D, et al. Quantum correlations between single telecom photons and a multimode on-demand solid-state quantum memory. Phys Rev X 2017;7:021028.
[33] Barreiro JT, Wei T-C, Kwiat PG. Beating the channel capacity limit for linear photonic superdense coding. Nat Phys 2008;4:282–6.
[34] Nicolas A, Veissier L, Giner L, et al. A quantum memory for orbital angular momentum photonic qubits. Nat Photonics 2014;8:234–8.
[35] Ding DS, Zhang W, Zhou ZY, et al. Quantum storage of orbital angular momentum entanglement in an atomic ensemble. Phys Rev Lett 2015;114:050502.
[36] Zhou ZQ, Hua YL, Liu X, et al. Quantum storage of three-dimensional orbital-angular-momentum entanglement in a crystal. Phys Rev Lett 2015;115:070502.
[37] Ou ZY, Lu YJ. Cavity enhanced spontaneous parametric down-conversion for the prolongation of correlation time between conjugate photons. Phys Rev Lett 1999;83:2556–9.
[38] Drever RWP, Hall JL, Kowalski FV, et al. Laser phase and frequency stabilization using an optical resonator. Appl Phys B 1983;31:97.
[39] Eckardt RC, Nabors CD, Kozlovsky WJ, et al. Optical parametric oscillator frequency tuning and control. J Opt Soc Am B 1991;8:646–67.
[40] Luo KH, Herrmann H, Krapick S, et al. Direct generation of genuine single-longitudinal-mode narrowband photon pairs. New J Phys 2015;17:073039.
[41] Wang FY, Shi BS, Zhai C, et al. Experimental measuring of the coherence length of a single photon generated via a degenerated optical parametric oscillator far below threshold. J Mod Optic 2010;57:330–3.
[42] Yang TS, Zhou ZQ, Hua YL, et al. Multiplexed storage and real-time manipulation based on a multiple degree-of-freedom quantum memory. Nat Commun 2018;9:3407.
[43] Zhou ZY, Li Y, Ding D-S, et al. Tunable cavity-enhanced photon pairs source in Hermite-Gaussian mode. AIP Adv 2016;6:025114.
[44] Clausen C, Bussieres F, Afzelius M, et al. Quantum storage of heralded polarization qubits in birefringent and anisotropically absorbing materials. Phys Rev Lett 2012;108:190503.
[45] Usmani I, Clausen C, Bussières F, et al. Heralded quantum entanglement between two crystals. Nat Photonics 2012;6:234–7.
[46] Bozinovic N, Yue Y, Ren Y, et al. Terabit-scale orbital angular momentum mode division multiplexing in fibers. Science 2013;340:1545–8.
[47] Wang J, Yang JY, Fazal IM, et al. Terabit free-space data transmission employing orbital angular momentum multiplexing. Nat Photonics 2012;6:488–96.
[48] Sit A, Bouchard F, Fickler R, et al. High-dimensional intracity quantum cryptography with structured photons. Optica 2017;4:1006.
[49] Afzelius M, Simon C, de Riedmatten H, et al. Multimode quantum memory based on atomic frequency combs. Phys Rev A 2009;79:052329.
[50] Tang JS, Zhou ZQ, Wang YT, et al. Storage of multiple single-photon pulses emitted from a quantum dot in a solid-state quantum memory. Nat Commun 2015;6:8652.
[51] Sinclair N, Saglamyurek E, Mallahzadeh H, et al. Spectral multiplexing for scalable quantum photonics using an atomic frequency comb quantum memory and feed-forward control. Phys Rev Lett 2014;113:053603.
[52] Saglamyurek E, Grimau Puigibert M, Zhou Q, et al. A multiplexed light-matter interface for fibre-based quantum networks. Nat Commun 2016;7:11202.
[53] Huang H, Milione G, Lavery MP, et al. Mode division multiplexing using an orbital angular momentum mode sorter and MIMO-DSP over a graded-index few-mode optical fibre. Sci Rep 2015;5:14931.
[54] Krenn M, Handsteiner J, Fink M, et al. Twisted light transmission over 143 km. Proc Natl Acad Sci USA 2016;113:13648–53.

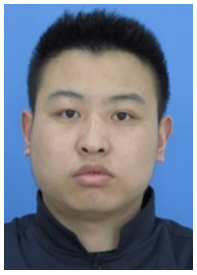

Yi-Lin Hua is now an assistant Research Fellow of Shanghai Institute of Laser Plasma, China Academy of Engineering Physics. He received his Ph.D. degree (2018) from University of Science and Technology of China. He is now interested in narrowband quantum light source for quantum memory and the research of high-power laser.

Zong-Quan Zhou is an associate professor of University of Science and Technology of China. He received his Ph.D. degree (2015) from University of Science and Technology of China. He is now mainly focusing on the experimental investigation on quantum information and quantum physics based on the solid-state quantum memory.

Chuan-Feng Li is a professor in University of Science and Technology of China. He received his Ph.D. degree (1999) from University of Science and Technology of China. His research field is quantum optics and quantum information. He is now focusing on constructing quantum network and exploring quantum physics with quantum technology.